Sum rules and physical bounds for a particulate slab --- transmission

Kristensson, Gerhard

2023

Document Version:
Publisher's PDF, also known as Version of record

CODEN:LUTEDX/(TEAT-7279)/1-29/(2023)
Revision No. 2: March 2024

Sum rules and physical bounds for a particulate slab—transmission

Gerhard Kristensson

Electromagnetic Theory
Department of Electrical and Information Technology
Lund University
Sweden

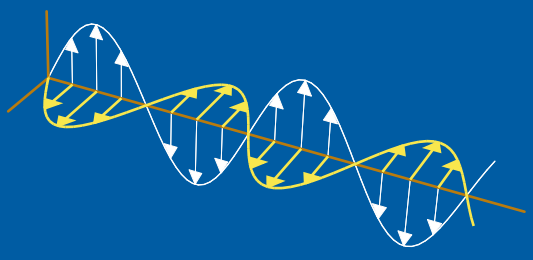

(TEAT-7279)/1-29/(2023): G. Kristensson, Sum rules a collection of randomly located obstacles—transmission

Gerhard Kristensson
gerhard.kristensson@eit.lth.se

Department of Electrical and Information Technology
Electromagnetics and Nanoelectronics
Lund University
P.O. Box 118
SE-221 00 Lund
Sweden

Editor: Mats Gustafsson

Abstract

Two different sum rules for transmission of the coherent electromagnetic field by a particulate slab are established. The particles are assumed spherical and randomly located, and the slab is illuminated by a plane wave at normal incidence. These sum rules are obtained assuming the particles are passive scatterers, and satisfy energy conservation and causality conditions. The sum rules are then employed to generate physical bounds on a combination of the bandwidth and a given transmission level. A potential check of the accuracy of the numerical computations is also admitted by the exact sum rules. A series of numerical computations illustrates the results obtained in the paper.

1 Introduction

In recent years, many useful sum rules and physical bounds have been developed for electromagnetic applications. Examples of these applications are radar absorbers [23], periodic structures (frequency selective surfaces) [7, 19], passive scatterers [25], antennas [5], metamaterials [4], near-zero material, and high-impedance surfaces [2, 6]. The underlying mathematical theory behind the sum rules is covered by many authors [1, 20]. These references also contain additional, relevant literature on the topic.

The reflected and transmitted fields by a particulate slab consist of a coherent (averaged) part and an incoherent part. In this paper, we develop two sum rules and corresponding physical bounds for the coherent transmitted electromagnetic field by a particulate slab. One main question of this paper is to find a limit or to predict the bandwidth of the coherent transmitted field for a given transmission level. To answer this question, we use the obtained physical bounds. The underlying theory and the numerical implementation of the coherent reflected and transmitted fields by a random collection of particles in a slab geometry are very well investigated in a series of paper [8, 9, 12, 15–18].

The calculation of the transmission coefficient by a slab is reviewed in Section 2, and in Section 3, the analytic properties of the transmission coefficient are analyzed. This section also contains two sum rules and physical bounds of the transmission coefficient of the coherent field. A few numerical examples are presented in Section 4, and the results are summarized in Section 5. A series of appendices concludes the paper.

2 Coherent transmitted field by a particulate slab

The geometry of the problem is depicted in Figure 1, and for the application in this paper, we specialize to an incident plane wave at normal incidence polarized in the x-direction, *i.e.*,

$$\boldsymbol{E}_{\mathrm{i}}(z) = \boldsymbol{E}_0 \mathrm{e}^{\mathrm{i}kz} = E_0 \hat{\boldsymbol{x}} \mathrm{e}^{\mathrm{i}kz}$$

For simplicity and to fix ideas, we assume all particles are identical. The particles can be a homogeneous spherical particle or a radially layered dielectric particle.

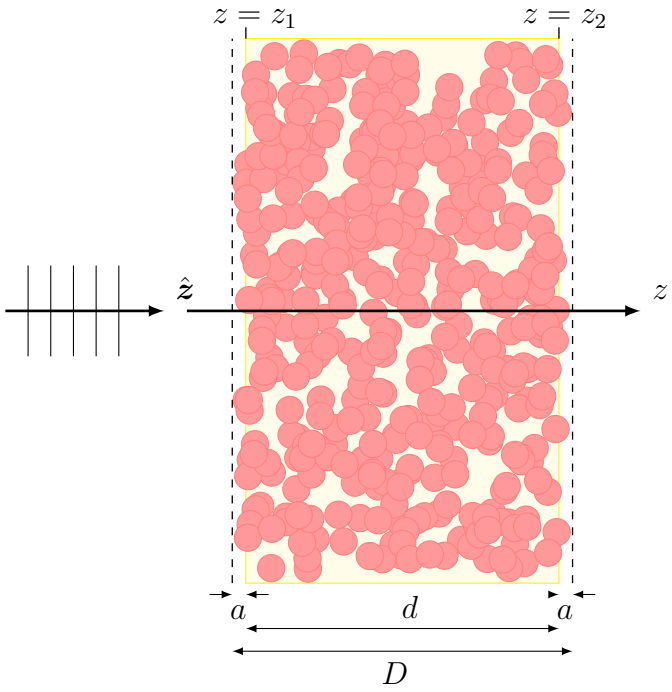

Figure 1: The geometry of the material region $z \in [z_1 - a, z_2 + a]$. In three dimensions, the spheres do not intersect. However, in this two-dimensional graph some of the projections of the spheres overlap. The yellow region denotes the region of possible locations of local origins, *i.e.*, the interval $[z_1, z_2]$.

Optically active materials are excluded. The common radius of the particles is denoted a. Generalizations of these assumptions are possible. The N particles are assumed indistinguishable.

The material is confined to the slab $z \in [z_1 - a, z_2 + a]$, and we adopt the notation $d = z_2 - z_1$ and $D = d + 2a$. Note the difference between the slab containing the local origins, $[z_1, z_2]$ (thickness d), and the material confinement, $[z_1 - a, z_2 + a]$ (thickness D), see Figure 1.

The expressions of the total coherent (average) fields on both sides of the slab for an incident plane wave are [12]

$$\langle \boldsymbol{E}_{\rm r}(z) \rangle = r(k) \boldsymbol{E}_0 {\rm e}^{-{\rm i}kz}, \quad z < z_1 - a, \qquad \langle \boldsymbol{E}_{\rm t}(z) \rangle = t(k) \boldsymbol{E}_0 {\rm e}^{{\rm i}kz}, \quad z > z_2 + a$$

where $r(k)$ and $t(k)$ are the reflection and transmission coefficients of the slab, respectively.

The transmission coefficient $t(k)$ of the slab is [11, 12][1]

$$t(k) = 1 + \frac{2\pi n_0}{k^3 E_0} \sum_{\tau=1}^{2} \sum_{l=1}^{\infty} {\rm i}^{-l+\tau-1} \sqrt{\frac{2l+1}{8\pi}} y_{\tau l}(k) \tag{2.1}$$

[1]The reflection coefficient $r(k)$ is computed in a similar manner [12], but we do not give the details here, since focus is on the transmitted field.

where

$$y_{\tau l}(k) = k \int_{z_1}^{z_2} \mathrm{e}^{-\mathrm{i}kz'} f_{\tau l}(z') \, \mathrm{d}z' \tag{2.2}$$

The number density of the particles is denoted n_0. The volume fraction of the particles φ and the number density n_0 are related by [17]

$$\varphi = n_0 \frac{4\pi a^3}{3} \left(1 - \frac{2a}{D}\right) = n_0 \frac{4\pi a^3}{3} \frac{d}{D} \tag{2.3}$$

Under the assumption of the Quasi Crystalline Approximation (QCA), the coefficients $f_{\tau l}(z)$ satisfy the following system of integral equations [12]:

$$\begin{aligned} f_{\tau l}(z) &= t_{\tau l} \mathrm{i}^{l-\tau+1} \sqrt{2\pi(2l+1)} E_0 \mathrm{e}^{\mathrm{i}kz} \\ &\quad + \frac{n_0}{k^2} t_{\tau l} \sum_{\tau'=1}^{2} \sum_{l'=1}^{\infty} \int_{z_1}^{z_2} K_{\tau l \tau' l'}(z - z') f_{\tau' l'}(z') \, \mathrm{d}z', \quad z \in [z_1, z_2] \end{aligned} \tag{2.4}$$

where the transition matrix of the particles are denoted $t_{\tau l}$, and the kernel $K_{\tau l \tau' l'}(z)$ has the form [11, 12]

$$K_{\tau l \tau' l'}(z) = \sum_{\lambda=|l-l'|+|\tau-\tau'|}^{l+l'} \mathcal{A}_{\tau l \tau' l' \lambda} I_\lambda(-kz, 2ka) \tag{2.5}$$

where the real numbers $\mathcal{A}_{\tau l \tau' l' \lambda}$ are calculated in [12], and the values are explicitly given in Appendix A. The integrals $I_\lambda(kz, \eta)$ are

$$I_\lambda(\zeta, \eta) = \int_{b(\zeta)}^{\infty} g(\sqrt{x^2 + \zeta^2}) \mathrm{h}_l^{(1)}(\sqrt{x^2 + \zeta^2}) \mathrm{P}_l(\zeta / \sqrt{x^2 + \zeta^2}) x \, \mathrm{d}x, \quad \zeta \in \mathbb{R}$$

where

$$b(\zeta) = \begin{cases} \sqrt{\eta^2 - \zeta^2}, & -\eta \le \zeta \le \eta \\ 0, & |\zeta| > \eta \end{cases}$$

and $g(r)$ is the pair correlation function. These integrals have a closed form solution for the hole correction (HC), *i.e.*, when $g(r) = \mathrm{H(r - 2a)}$, see [13]. The exact expression of the integral $I_\lambda(\zeta, \eta)$ is reviewed in boxed Note 1 below.

The procedure outline above solves the transmission problem for the coherent (average) field exactly and includes all interaction effects between the particles. For a given configuration (geometry, material parameters, and number density) compute the solution $f_{\tau l}(z)$ to the system of integral equations in (2.4). Proceed by computing the coefficient $y_{\tau l}(k)$ in (2.2), and, finally, sum the terms in (2.1) to get the transmission coefficient $t(k)$.

1. Evaluation of the function $I_l(\zeta,\eta)$

Some effective ways to compute the integrals $I_l(\zeta,\eta)$, $\zeta\in\mathbb{R}$, $\eta\in\mathbb{R}$, $l=0,1,2,\ldots$, for the hole correction (HC), are presented in [13]. The definition of the integral is:

$$I_l(\zeta,\eta)=\int_0^\infty \mathrm{H}(\sqrt{x^2+\zeta^2}-\eta)\mathrm{h}_l^{(1)}(\sqrt{x^2+\zeta^2})\mathrm{P}_l(\zeta/\sqrt{x^2+\zeta^2})x\,\mathrm{d}x$$

The result is

$$I_l(\zeta,\eta)=\mathrm{i}^l\mathrm{e}^{-\mathrm{i}\zeta},\quad \zeta\le-\eta,\qquad I_l(\zeta,\eta)=\mathrm{i}^{-l}\mathrm{e}^{\mathrm{i}\zeta},\quad \zeta\ge\eta$$

and

$$I_l(\zeta,\eta)=-\eta\mathrm{h}_{l+1}^{(1)}(\eta)\mathrm{P}_l(\zeta/\eta)+\sum_{k=0}^{[l/2]}(-1)^k(2l-4k+1)\mathrm{h}_{l-2k}^{(1)}(\eta)\mathrm{P}_{l-2k}(\zeta/\eta),\quad \zeta\in(-\eta,\eta)$$

which is a finite sum of spherical waves.

A useful property of the $I_l(\zeta,\eta)$ function is the parity property: $I_l(-\zeta,\eta)=(-1)^lI_l(\zeta,\eta)$.

2.1 Low-frequency behaviour

The low-frequency expression of the transmission coefficient for spherical particles of radius a is, see Appendix B

$$t(k)=1+9\varphi kD\left(\frac{t_{11}}{4(ka)^3+6\mathrm{i}\varphi t_{11}\frac{D}{d}}+\frac{t_{21}}{4(ka)^3+6\mathrm{i}\varphi t_{21}\frac{D}{d}}\right)+\mathrm{i}kH^{\mathrm{Corr}}\tag{2.6}$$

where the transition matrix of the spherical particle is denoted $t_{\tau l}$. The real-valued coefficient H^{Corr} is a small correction term,[2] see (B.1) in Appendix B. In most situations, the correction term has no practical importance, but becomes important when high precision is required, see Section 4.2. Note that (2.6) is the low-frequency expression of the transmission coefficient under the assumption of the hole correction (HC) pair correlation function. Note also that the low-frequency limit in (2.6) is not the identical to the homogenization limit, which also requires $a/D\to0$.

2.1.1 Non-magnetic dielectric sphere

If the spherical particles are non-magnetic, $\mu=1$, and with a permittivity ϵ_1, then $t_{11}=0$ (to leading order in ka) and to leading order in powers of ka

$$t_{21}=\frac{2\mathrm{i}(ka)^3}{3}y+O\left((ka)^5\right)$$

[2] In the numerical illustrations in Section 4 the contribution is approximately 0.3%.

Spherical particle	**Coefficient** H
Perfectly conducting	$\frac{3\varphi D}{2}\frac{1+2\varphi\frac{D}{d}}{(1-\varphi\frac{D}{d})(2+\varphi\frac{D}{d})}+H^{\text{Corr}}$
Non-magnetic dielectric	$\frac{3\varphi D}{2}\frac{y}{1-\varphi y\frac{D}{d}}+H^{\text{Corr}}$ $H^{\text{Corr}}=\frac{24\varphi y D a}{d}\left(\int_0^1\frac{\mathrm{d}t}{4-\varphi y\frac{D}{d}(2+3t-t^3)}-\frac{1}{4-4\varphi y\frac{D}{d}}\right)$

Table 1: The constant H for different spherical particles with HC. The small correction term is explicitly given in Appendix B.

where

$$y=\frac{\epsilon_1-\epsilon}{\epsilon_1+2\epsilon}$$

The constant y can also be written in terms of the polarizability γ_{e} of the particle [14, Sec. 7.9].

$$\gamma_{\text{e}}=4\pi a^3 y$$

To leading order in powers of ka, the transmission coefficients $t(k)$ for spherical, non-magnetic, homogeneous particles with HC is

$$t(k)=1+\frac{3\mathrm{i}\varphi kD}{2}\frac{y}{1-\varphi y\frac{D}{d}}+H_2^{\text{Corr}}$$

To leading order in powers of ka, we summarize the behaviour of the transmission coefficients $t(k)$ as

$$t(k)=1+\mathrm{i}kH+O((ka)^2)$$

where H is a real-valued coefficient of dimension length, and its value for different particles with HC is collected in Table 1. Numerical calculations show that the difference between H in Table 1, obtained with the hole correction, and the Percus-Yevick approximation is small, see also [17]. We neglect any differences of the effect of the pair correlation function, and use the expression of H in Table 1. Note that these low-frequency expressions are not the same as the homogenization expressions, which corresponds to letting $a/d\to 0$ (or $D/d\to 1$). In the low-frequency limit $k\to 0$, the structure of the slab remains, *i.e.*, $a/d=$ constant, and the medium is not homogeneous. In the homogenization limit, $H^{\text{Corr}}\to 0$ and $D/d\to 1$.

3 Analytic properties of the transmission coefficient

In this section, the analytic properties of the transmission coefficient of a slab, filled with passive particles, are investigated. Some relevant literature on the topic is found in [1, 4, 6, 7, 19, 20].

3.1 Causality

In a time-domain setting, a general incident wave of fixed polarization $\hat{\boldsymbol{x}}$ impinges on a slab $z \in [z_1 - a, z_2 + a]$. The background wave velocity is c and the wavenumber is denoted $k = \omega/c$. We have

$$\boldsymbol{E}_{\mathrm{i}}(z,t) = \hat{\boldsymbol{x}} \int_{-\infty}^{\infty} A(k) \mathrm{e}^{\mathrm{i}kc((z-z_1+a)/c-t)} \,\mathrm{d}k, \qquad z < z_1 - a$$

We assume the incident field $\boldsymbol{E}_{\mathrm{i}}(z_1 - a, t) = 0$, $t < 0$ and that $A(k) \in L^2(\mathbb{R})$. This implies by Titchmarsh's theorem [1, 21] that $A(k)$ is analytic in the upper complex plane $\mathbb{C}_+ = \{z \in \mathbb{C} : \operatorname{Im} z > 0\}$. The amplitude $A(k)$ is not only in $L^2(\mathbb{R})$ for an argument on the real axis. It is also in $L^2(\mathbb{R})$ on every line in the upper half plane parallel to the real axis. The reflected and transmitted fields are

$$\begin{cases} \boldsymbol{E}_{\mathrm{r}}(z,t) = \hat{\boldsymbol{x}} \displaystyle\int_{-\infty}^{\infty} r(k) A(k) \mathrm{e}^{-\mathrm{i}kc((z-z_1+a)/c+t)} \,\mathrm{d}k, & z < z_1 - a \\ \boldsymbol{E}_{\mathrm{t}}(z,t) = \hat{\boldsymbol{x}} \displaystyle\int_{-\infty}^{\infty} \mathrm{e}^{\mathrm{i}kD} t(k) A(k) \mathrm{e}^{\mathrm{i}kc((z-z_2-a)/c-t)} \,\mathrm{d}k, & z > z_2 + a \end{cases}$$

where $D = z_2 - z_1 + 2a$. The fields $\boldsymbol{E}_{\mathrm{i}}(z,t)$, $\boldsymbol{E}_{\mathrm{r}}(z,t)$, and $\boldsymbol{E}_{\mathrm{t}}(z,t)$ are real quantities, which imply

$$A(k) = A^*(-k), \quad r(k) = r^*(-k), \quad t(k) = t^*(-k), \quad k \in \mathbb{R}$$

Moreover, by causality, $\boldsymbol{E}_{\mathrm{r}}(z_1 - a, t) = 0$, $t < 0$ and $\boldsymbol{E}_{\mathrm{t}}(z_2 + a, t) = 0$, $t < 0$.[3] This implies that $r(k)$ and $t_D(k) = \mathrm{e}^{\mathrm{i}kD} t(k)$ have analytic continuations in $\mathbb{C}_+$ [21].

On the real axis, energy conservation, $|r(k)|^2 + |t(k)|^2 \le 1$, implies, $|r(k)| \le 1$ and $|t_D(k)| = |t(k)| \le 1$. In $\mathbb{C}_+$, we have by Cauchy's theorem (note that $t_D A \in L^2(\mathbb{R})$ if $A \in L^2(\mathbb{R})$) [21]

$$t_D(\kappa) A(\kappa) = \frac{1}{2\pi\mathrm{i}} \int_{-\infty}^{\infty} \frac{t_D(k') A(k')}{k' - \kappa} \,\mathrm{d}k', \quad \kappa \in \mathbb{C}_+$$

and

$$|t_D(\kappa)| \le \frac{1}{2\pi |A(\kappa)|} \int_{-\infty}^{\infty} \frac{|A(k')|}{|k' - \kappa|} \,\mathrm{d}k', \quad \kappa \in \mathbb{C}_+$$

Let $\kappa_1 = k_1 + \mathrm{i}\varsigma_1$, $\varsigma_1 > 0$, and $A(\kappa) = 1/(\kappa - \kappa_1^*) = 1/(\kappa - k_1 + \mathrm{i}\varsigma_1)$, which is a causal transform and belongs to $L^2(\mathbb{R})$.

$$|t_D(\kappa_1)| \le \frac{\varsigma_1}{\pi} \int_{-\infty}^{\infty} \frac{1|}{\sqrt{(k' - k_1)^2 + \varsigma_1^2}} \,\mathrm{d}k' = 1, \quad \kappa_1 \in \mathbb{C}_+$$

and we get

$$|t_D(\kappa)| \le 1, \quad \kappa \in \mathbb{C}_+ \cup \mathbb{R}$$

[3] This formulation of causality is unnecessarily strong. A weaker formulation is also adopted below.

The dispersion relation for a causal function $f(\zeta)$ (analytic and bounded in $\mathbb{C}_+$) with one subtraction reads (for details, see [21])

$$\begin{cases} f(\kappa) = f(0) + \dfrac{\kappa}{2\pi \mathrm{i}} \fint_{-\infty}^{\infty} \dfrac{f(k') - f(0)}{k'(k' - \kappa)} \, \mathrm{d}k', & \operatorname{Im} \kappa > 0 \\ f(k) = f(0) + \dfrac{k}{\pi \mathrm{i}} \fint_{-\infty}^{\infty} \dfrac{f(k') - f(0)}{k'(k' - k)} \, \mathrm{d}k', & k \in \mathbb{R} \end{cases}$$

where $\fint$ denotes the Cauchy's principal value. Apply to $t_D(k)$. Since $t_D(0) = 1$, we get

$$\begin{cases} \operatorname{Re}\left(\mathrm{e}^{\mathrm{i}kD} t(k)\right) = 1 + \dfrac{k}{\pi} \fint_{-\infty}^{\infty} \dfrac{\operatorname{Im}\left(\mathrm{e}^{\mathrm{i}kD} t(k')\right)}{k'(k' - k)} \, \mathrm{d}k' \\ \operatorname{Im}\left(\mathrm{e}^{\mathrm{i}kD} t(k)\right) = -\dfrac{k}{\pi} \fint_{-\infty}^{\infty} \dfrac{\operatorname{Re}\left(\mathrm{e}^{\mathrm{i}kD} t(k')\right) - 1}{k'(k' - k)} \, \mathrm{d}k' \end{cases} \qquad k \in \mathbb{R}$$

We notice that the sum rule holds for $t_D(k)$ and not for $t(k)$. This is due to the necessary time shift $\mathrm{e}^{\mathrm{i}kD}$. If we assume the wave front velocity in the slab does not exceed c, we can apply a weaker form of causality, $\boldsymbol{E}_{\mathrm{t}}(z_2 + a, t + D/c) = 0$, $t < 0$.[4]

$$\begin{cases} \boldsymbol{E}_{\mathrm{i}}(z_1 - a, t) = \hat{\boldsymbol{x}} \displaystyle\int_{-\infty}^{\infty} A(k) \mathrm{e}^{-\mathrm{i}kct} \, \mathrm{d}k \\ \boldsymbol{E}_{\mathrm{t}}(z_2 + a, t + D/c) = \hat{\boldsymbol{x}} \displaystyle\int_{-\infty}^{\infty} t(k) A(k) \mathrm{e}^{-\mathrm{i}kct} \, \mathrm{d}k \end{cases}$$

and we can proceed as above, but with $t(k)$ instead of $t_D(k)$. We conclude that $t(k)$ is analytic in $\mathbb{C}_+$ and $|t(\kappa)| \leq 1$ in $\mathbb{C}_+ \cup \mathbb{R}$. Since $t(0) = 1$, we get

$$\begin{cases} \operatorname{Re} t(k) = 1 + \dfrac{k}{\pi} \fint_{-\infty}^{\infty} \dfrac{\operatorname{Im} t(k')}{k'(k' - k)} \, \mathrm{d}k' \\ \operatorname{Im} t(k) = -\dfrac{k}{\pi} \fint_{-\infty}^{\infty} \dfrac{\operatorname{Re} t(k') - 1}{k'(k' - k)} \, \mathrm{d}k' \end{cases} \qquad k \in \mathbb{R}$$

We notice that knowledge of the imaginary part of the transmission coefficient on the entire real axis determines its real part and *vice versa*. In the sections below, we derive other, more useful, sum rules based upon the logarithm.

3.2 Sum rule with the logarithm

Construct a Herglotz function $h_1(\kappa)$, see Appendix D for definition, from the transmission coefficient $t(\kappa)$. Following [7], we obtain in an appropriately chosen branch of the logarithm

$$h_1(\kappa) = -\mathrm{i} \ln \left(t(\kappa) \prod_{n=1}^{N} \frac{1 - \kappa/\kappa_n^*}{1 - \kappa/\kappa_n} \right)$$

[4] This assumption excludes the case with particles having internal wave speed higher than the background wave speed.

where κ_n, $n = 1, 2, \ldots, N$, are the zeros of the transmission coefficient $t(\kappa)$ in the upper complex plane $\mathbb{C}_+$, *i.e.*, $\operatorname{Im} \kappa_n > 0$, $n = 1, 2, \ldots, N$. The product is called a Blaschke product [24]. Note that for real k, all terms in the product have modulus one, *i.e.*,

$$\left| \frac{1 - k/\kappa_n^*}{1 - k/\kappa_n} \right| = 1, \quad k \in \mathbb{R}$$

and

$$\operatorname{Im} h_1(k) = -\operatorname{Re} \ln \left(t(k) \prod_{n=1}^{N} \frac{1 - k/\kappa_n^*}{1 - k/\kappa_n} \right) = -\ln |t(k)|, \quad k \in \mathbb{R}$$

and $\operatorname{Im} h_1(k)$ is an even function of the real argument k.

The low-frequency behavior of $h_1(k)$ becomes

$$\begin{aligned} h_1(k) &= -\mathrm{i} \left(\ln t(k) + \sum_{n=1}^{N} \ln (1 - k/\kappa_n^*) - \sum_{n=1}^{N} \ln (1 - k/\kappa_n) \right) \\ &= -\mathrm{i} \left(\mathrm{i}kH + k \sum_{n=1}^{N} \left(\frac{1}{\kappa_n} - \frac{1}{\kappa_n^*} \right) + o(k) \right) = kH + 2k \sum_{n=1}^{N} \operatorname{Im} \frac{1}{\kappa_n} + o(k) \end{aligned}$$

where H has dimension length. With the notation introduced in Appendix D, the asymptotic expansion at $z = 0$ is of order $N_0 = 1$, and $a_{-1} = a_0 = 0$, $a_1 = H + 2 \sum_{n=1}^{N} \operatorname{Im} \frac{1}{\kappa_n}$.

At high frequencies, under the assumption that transmission has a limit value t_∞, we have

$$h_1(k) = o(k)$$

With the notation of Appendix D, the asymptotic expansion at $z = \infty$ is of order $N_\infty = -1$, and $b_1 = 0$.

Consequently, see Theorem D.2 in Appendix D

$$-\frac{2}{\pi} \int_0^\infty \frac{\ln |t(k)|}{k^2} \, \mathrm{d}k = \frac{2}{\pi} \int_0^\infty \frac{\operatorname{Im} h_1(k)}{k^2} \, \mathrm{d}k = H + 2 \sum_{n=1}^{N} \operatorname{Im} \frac{1}{\kappa_n} \leq H$$

The integral is well-behaved. This is the exact value of the sum rule. The sum rule as an integral in $\lambda = 2\pi/k$ reads

$$\int_0^\infty \ln \frac{1}{|t(\lambda)|} \, \mathrm{d}\lambda = -\int_0^\infty \ln |t(\lambda)| \, \mathrm{d}\lambda = -2\pi \int_0^\infty \frac{\ln |t(k)|}{k^2} \, \mathrm{d}k \leq \pi^2 H \tag{3.1}$$

In the next subsection, we use this sum rule to find bounds on the product of the bandwidth and the prescribed transmission rate.

3.2.1 Physical bound

Estimate the left-hand side of the wavelength integral in (3.1) from below. For a given transmission level $t_0 \in (0, 1]$, let $I(t_0)$ be the interval of wavelength where transmission is less than t_0, *i.e.*, $|t(\lambda)| \le t_0 \le 1$, $\lambda \in I(t_0)$. The interval $I(t_0)$ can consist of a union of disjoint parts. Then, since the integrand in (3.1) is a positive function, a crude estimate is

$$|I(t_0)| \ln \frac{1}{t_0} \le \int_{I(t_0)} \ln \frac{1}{|t(\lambda)|}\, \mathrm{d}\lambda \le \int_0^\infty \ln \frac{1}{|t(\lambda)|}\, \mathrm{d}\lambda \le \pi^2 H$$

where $|I(t_0)|$ denotes the length of the interval $I_0(t_0)$. We get the physical bound

$$\boxed{|I(t_0)| \le \frac{\pi^2 H}{\ln \frac{1}{t_0}} = \frac{\pi^2 H}{|\ln t_0|}} \tag{3.2}$$

A similar bound for a periodic array has been reported in [7]. A numerical example of this physical bound is presented in Section 4.1.

3.3 Sum rule with pulse Herglotz function

A more elaborate Herglotz function is the pulse Herglotz function [20].

$$\boxed{h_\Delta(z) = -\frac{1}{\pi} \int_{-\Delta}^{\Delta} \frac{1}{z - t}\, \mathrm{d}t = \frac{1}{\pi} \ln \frac{z - \Delta}{z + \Delta}, \quad \operatorname{Im} z > 0}$$

where $\Delta > 0$, and the branch cut of the logarithm is assumed along the negative real axis. Details on this function are presented in Appendix E.

The asymptotes of $h_\Delta(z)$ are

$$h_\Delta(z) = \begin{cases} \mathrm{i} - \dfrac{2z}{\pi\Delta} + O(z^2), & z \hat{\to} 0 \\[2ex] -\dfrac{2\Delta}{z\pi} + O(z^{-2}), & z \hat{\to} \infty \end{cases}$$

The symbol $z \hat{\to} 0$ stands for the non-tangential limit $|z| \to 0$ within some Stoltz domain $\{z \in \mathbb{C}_+ : \theta \le \arg(z) \le \pi - \theta\}$ with the angle $\theta \in (0, \pi/2]$. For more details, see Appendix D.

The imaginary part of $h_\Delta(z)$ is non-negative and bounded by unity in the upper half plane $\mathbb{C}_+$. Specifically, the inner part of the circle $|z| = \Delta$ in the upper complex half plane maps to $1/2 < \operatorname{Im} h_\Delta(z) < 1$, see Figure 13. In the region outside the circle $|z| = \Delta$ in the upper complex half plane, we have $0 < \operatorname{Im} h_\Delta(z) < 1/2$.

The Möbius transformation

$$w(z) = \mathrm{i}\frac{1 + z}{1 - z} \quad \Leftrightarrow \quad z(w) = \frac{w - \mathrm{i}}{w + \mathrm{i}}$$

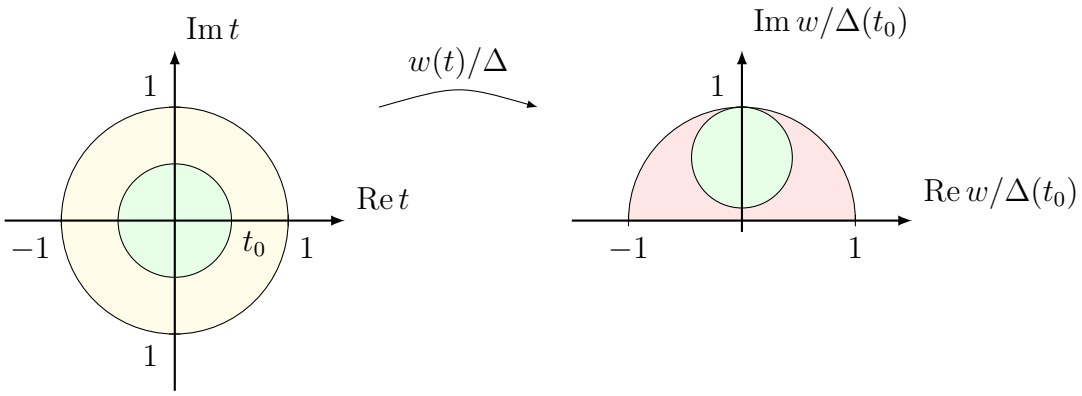

Figure 2: The Möbius transform $w(t)/\Delta$. The green circle is the image of $|t(k)| \leq t_0 = 0.5$.

maps the unit circle to the upper complex half plane. Moreover, a circle centered at the origin with radius $t_0 \in (0, 1]$ in the z-plane is mapped to a circle centered at $w_0 = \mathrm{i}(1 + t_0^2)/(1 - t_0^2)$ with radius $r_0 = 2t_0/(1 - t_0^2)$ in the w-plane.

Define the Herglotz function $h_2(\kappa) \stackrel{\text{def}}{=} h_\Delta(w(t(\kappa)))$. The asymptotes of $w(t(\kappa))$ are

$$w(t(\kappa)) = \begin{cases} -\dfrac{2}{\kappa H} + O(1), & \kappa \hat{\to} 0 \\ \mathrm{i}\dfrac{1 + t_\infty}{1 - t_\infty} + O(|\kappa|^{-1}), & \kappa \hat{\to} \infty \end{cases}$$

and

$$h_2(\kappa) \stackrel{\text{def}}{=} h_\Delta(w(t(\kappa))) = \begin{cases} \dfrac{\kappa \Delta H}{\pi} + O(|\kappa|^2), & \kappa \hat{\to} 0 \\ o(k), & \kappa \hat{\to} \infty \end{cases}$$

Note that $w(t(-k)) = w(t^*(k)) = -w^*(t(k))$ and $h_2(-k) = h_\Delta(-w^*(t(k)))$ for $k \in \mathbb{R}$. Since $h_\Delta(-z^*) = -h_\Delta^*(z)$, we get $h_2(-k) = -h_2^*(k)$ for $k \in \mathbb{R}$. With the notation in Appendix D, the asymptotic expansion at $z = 0$ is of order $N_0 = 1$, and $a_{-1} = a_0 = 0$, $a_1 = \Delta H/\pi$, and the asymptotic expansion at $z = \infty$ is of order $N_\infty = -1$, and $b_1 = 0$.

We now determine the value of the scale factor $\Delta = \Delta(t_0)$. The aim is to find bounds on the bandwidth for transmission $|t| \leq t_0 \in (0, 1]$. The connection between parameter $\Delta(t_0)$ and the suggested threshold $|t| = t_0 \leq 1$ is found by

$$\Delta(t_0) = \frac{1 + t_0^2}{1 - t_0^2} + \frac{2t_0}{1 - t_0^2} = \frac{1 + t_0}{1 - t_0} > 0$$

This choice of $\Delta(t_0)$ maps the circle $|t| \leq t_0$ to a circle in the w/Δ-plane centered at $\mathrm{i}(1 + t_0^2)/(1 + t_0)^2$ with radius $2t_0/(1 + t_0)^2$ (green discs in Figure 2).

Consequently, see Theorem D.2 in Appendix D

$$\frac{2}{\pi}\int_0^\infty \frac{\operatorname{Im} h_2(k)}{k^2}\,\mathrm{d}k = \frac{\Delta H}{\pi} = \frac{1+t_0}{1-t_0}\frac{H}{\pi} \tag{3.3}$$

The integral is well-behaved. The sum rule as an integral in $\lambda = 2\pi/k$ reads

$$\boxed{\int_0^\infty \operatorname{Im} h_2(\lambda)\,\mathrm{d}\lambda = 2\pi\int_0^\infty \frac{\operatorname{Im} h_2(k)}{k^2}\,\mathrm{d}k = \pi\Delta H = \pi\frac{1+t_0}{1-t_0}H} \tag{3.4}$$

This is the exact value of the sum rule with the pulse Herglotz function. Note that for a given configuration, *i.e.*, given constant H, the sum rule holds for all transmission levels t_0.

In the next subsection, we use this sum rule to find a bound on the bandwidth given a certain transmission rate. The sum rule is exact and it can be used to verify the numerical computations of the transmission coefficient. In fact, for a given particle and transmission rate t_0, the right-hand side of (3.4) is given, and the integral on the left-hand side is determined.

3.3.1 Physical bound

We now apply the exact sum rule in (3.4) to get a physical bound on the bandwidth of the transmission coefficient, given a certain threshold $t_0 \in (0, 1]$. Let the wavelength interval $I(t_0)$ denote the interval where $|t| \leq t_0$. The interval $I(t_0)$ can consist of a union of disjoint parts. In this interval, the integrand is larger than $1/2$ by construction, and we get by estimating the integral

$$\frac{|I(t_0)|}{2} \leq \int_{I(t_0)} \operatorname{Im} h_2(\lambda)\,\mathrm{d}\lambda \leq \int_0^\infty \operatorname{Im} h_2(\lambda)\,\mathrm{d}\lambda = \pi\frac{1+t_0}{1-t_0}H$$

where $|I(t_0)|$, which is related to the bandwidth of the problem, denotes the length of the interval $I(t_0)$. In summary, we get

$$\boxed{|I(t_0)| \leq 2\pi\frac{1+t_0}{1-t_0}H} \tag{3.5}$$

A numerical example of this physical bound is presented in Section 4.2.

4 Numerical results

In a series of numerical examples, we illustrate the results in this paper.

4.1 First physical bound

We start with the physical bound obtained in Section 3.2. In Figures 3 and 4, the modulus and the negative logarithm of the modulus of the transmission coefficient, respectively, are depicted as a function of the scaled wavelength λ/a. In all figures[5] presented in this paper, the dielectric, spherical particles of radius a have permittivity $\epsilon_1/\epsilon = 4$, and permeability $\mu_1/\mu = 1$, the slab has thickness $D/a = 20$, and the volume fraction is $\varphi = 15\%$.

The value of the transmission coefficients in the complex plane as a function of λ/a along the curve is shown in Figure 5. We notice that the curve circles around the origin, which indicates that there are several zeros in the upper half plane [10, Th. 4.10a]. The exact behaviour at the origin is hard to ensure due to limited numerical precision at low transmission levels. Hence, the factor $\operatorname{Im} 1/\kappa_n$ is a strictly positive factor, that makes the sum rule in (3.1) less precise. The area under the entire curve in Figure 4 is approximately $20.8a$ while $\pi^2 H = 24.1a$. The gap between these two numbers also indicates that there are zeros in the upper complex half-plane. If we integrate over frequencies instead for over the wavelength, *i.e.*,

$$-\int_0^\infty \frac{\ln|t(k)|}{k^2}\,\mathrm{d}k \le \frac{\pi H}{2}$$

we obtain by numerical integration of the integral on the left-hand side $3.45a$, which should be compared with the value $\pi H/2 = 3.84a$.

At a transmission threshold of $t_0 = 0.5$, the right-hand side in (3.2) is calculated to $\pi^2 H/|\ln t_0| = 34.8a$. This value is much larger than the numerical value $|I(t_0)| \approx 5.3a$ obtained in the figure. However, this comes to no surprise, since the sum rule has to hold for all possible configurations, which have the same value of H and t_0. This illustration shows that our configuration is far from the extreme value. Whether this is good or bad depends on if the goal is high or low transmission rates for a large wavelength interval.

The bandwidth of the peak in Figure 4 can be estimated by the equating a box (red box in the figure) such that the area under the entire curve and of the box are the same ($\approx 20.8a$). More examples of estimating the bandwidth are presented in *e.g.*, [25]. The length of the wavelength interval of the red box is 1.63 in units of a.

4.2 Second physical bound

The Herglotz function, defined in Section 3.3, is depicted as a function of λ/a in Figure 6 for the same material data and geometry as in Section 4.1. Again, the transmission threshold is $t_0 = 0.5$. The argument w/Δ of the Herglotz function is shown in Figure 7. Note that the argument in the Herglotz function approaches the negative real axis from above as $\lambda/a \to \infty$.

An upper bound of the wavelength interval from (3.5) is $2\pi H\Delta(t_0) = 46.1a$, which is larger than the limit with the first physical bound in Section 3.2, and much larger than the value $|I(t_0)| \approx 5.3a$ obtained from the numerical example. Again,

[5] Figure 9 is an exception.

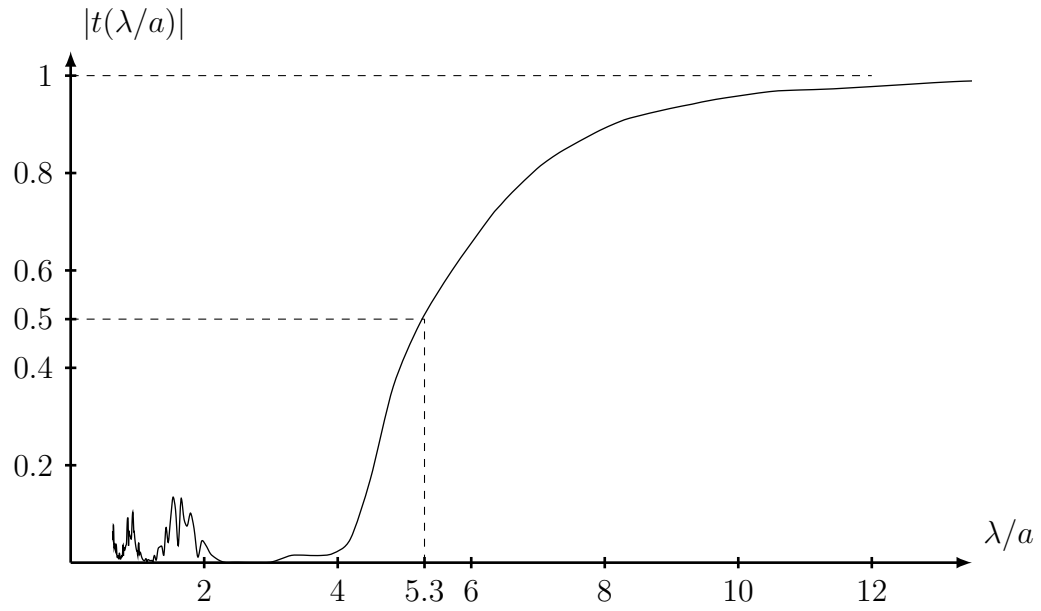

Figure 3: The absolute value of the transmission coefficient t as a function of the normalized wavelength λ/a for a slab of thickness $D/a = 20$, volume fraction $\varphi = 15\%$, permittivity $\epsilon_1/\epsilon = 4$, and permeability $\mu_1/\mu = 1$.

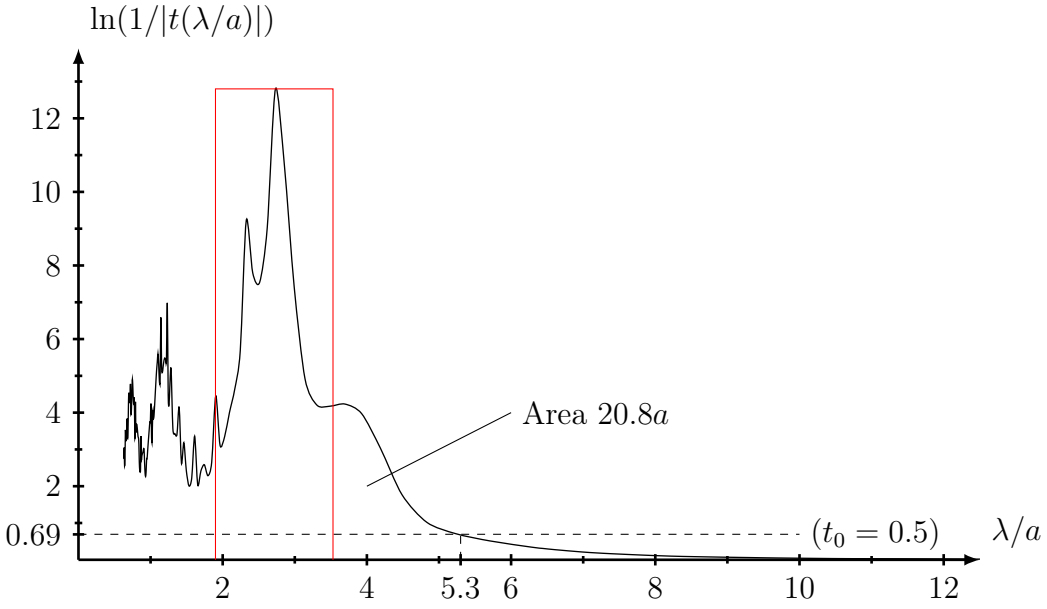

Figure 4: The function $\ln(1/|t|)$ as a function of the normalized wavelength λ/a for a slab of thickness $D/a = 20$, volume fraction $\varphi = 15\%$, permittivity $\epsilon_1/\epsilon = 4$, and permeability $\mu_1/\mu = 1$. The red box has the same area as the area under the curve ($\approx 20.8a$).

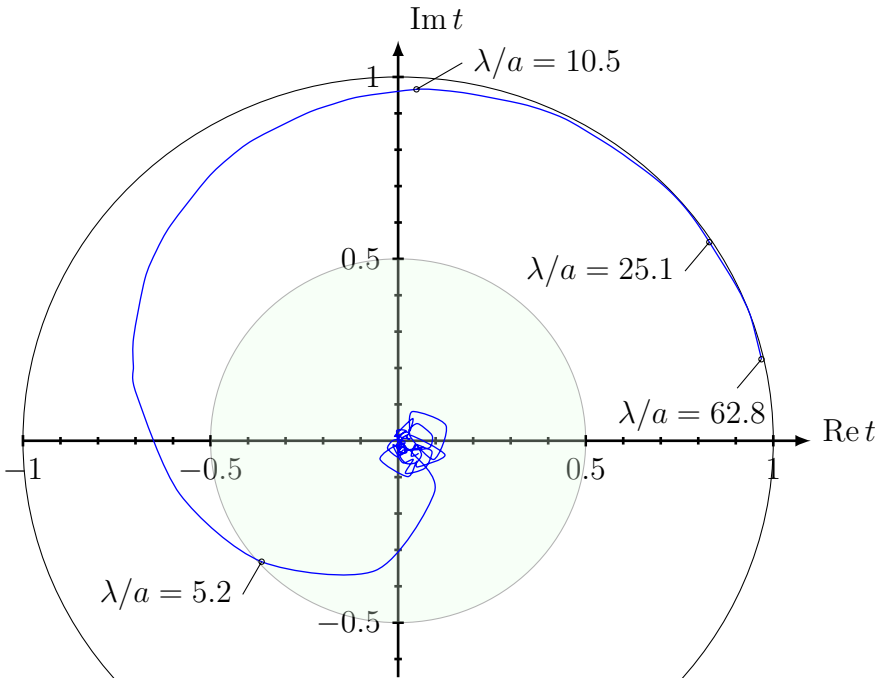

Figure 5: The components of the complex-valued transmission coefficient, t, in the complex plane as a function of the wavelength λ/a for a slab of thickness $D/a = 20$ and volume fraction $\varphi = 15\%$. The curve starts at $\lambda/a = 0$ at the origin and ends at 1 as $\lambda/a \to \infty$.

this is not surprising, since the sum rule holds for all possible configurations having the same value of H and t_0. If this is good or bad depends on whether a high or low transmission rate is requested.

Numerical integration of the area under the entire curve in Figure 6 gives a value of approximately $21.3a$. This value is smaller than the exact value $\pi H \Delta(t_0) = 23.0a$, which can be explained by loss of numerical procession at higher frequencies or the choice of numerical integration by the trapezoidal rule. As an alternative, we can instead integrate over normalized frequency ka, see (3.4), *i.e.*,

$$\int_0^\infty \frac{\operatorname{Im} h_2(ka)}{(ka)^2}\, \mathrm{d}ka = \frac{\Delta(t_0)H}{2a}$$

This form of the sum rule weights low frequencies higher and higher frequencies less, see Figure 8. Low frequency data have higher numerical precision, which guarantee a more accurate test of the sum rule. With the same data as above, the right-hand side is $\Delta(t_0)H/2 = 3.67a$, and the left-hand side is by numerical integration approximately $3.58a$. This is less than a 3% discrepancy, which is sufficient for most applications. A numerical test with different transmission levels $t_0 \in (0, 1)$ shows that the agreement gets better for higher values of t_0.

However, since the sum rule above is an exact identity, possible sources of error are important to identify. Some potential sources of this discrepancy are listed

Possible errors
Missing parts in the integration interval $[0, \infty)$
Appropriate numerical quadrature
Numerical solution of the system of integral equations
Correct pair correlation function—boundary effects
Effect of QCA

Table 2: Possible explanations of the discrepancies in the sum rule.

in Table 2. The integration is performed by both the trapezoidal and Simpson's rule over the interval $ka \in [0.00001, 8]$ (non-uniform points), which seems to suffice. Moreover, potential convergence problems in solving (2.4) have been eliminated by a comparison with an independent implementation [9]. Hence, with some confidence, we can eliminate these causes to the discrepancy.

However, a more likely cause, we find in the choice of the pair correlation function $g(r)$. We assume the pair correlation function (the Percus-Yevick approximation is employed) only depends on the distance between two particles, which definitely is an approximation of the correct pair correlation function, which depends on two points, *i.e.*, $g(\boldsymbol{r}, \boldsymbol{r}')$. Moreover, close to the boundary, there are effects that are not included in our choice of pair correlation function. How important these boundary effects are, we cannot estimate. A thicker slab should make these effects smaller, since then the boundary is a smaller portion of the slab geometry. Indeed, a computation with a thicker slab, $D/a = 100$ (all other parameters the same), confirms this conjecture, and the error is now 0.6%, see Figure 9.

The importance of the correct pair correlation is further emphasized if we compare the sum rule evaluated by the hole correction (HC) and the Percus-Yevick approximation (PY). The result is displayed in Figure 10, where numerical integration with the hole correction results in a large error in the evaluation of the sum rule. The hole correction seems not to generate a transmission coefficient that complies with energy conservation [16, 17], which seems to be the cause of the this huge discrepancy.

Finally, the Quasi Crystalline Approximation is assumed in the derivation of the system of integral equations. How this approximation affects the result, and whether the sum rule can be a test on this assumption is an open question.

5 Discussion and conclusions

Physical bounds on bandwidth and transmission rates are important tools in the design of slab configurations with specific transmission performance. In this paper, we have developed two different sum rules for the transmission coefficient. The particles of the slab are assumed to be passive, and the system has to satisfy causality and energy conservation. The sum rules are then employed to obtain physical bounds on the a combination of bandwidth and transmission rates. The exact sum rule

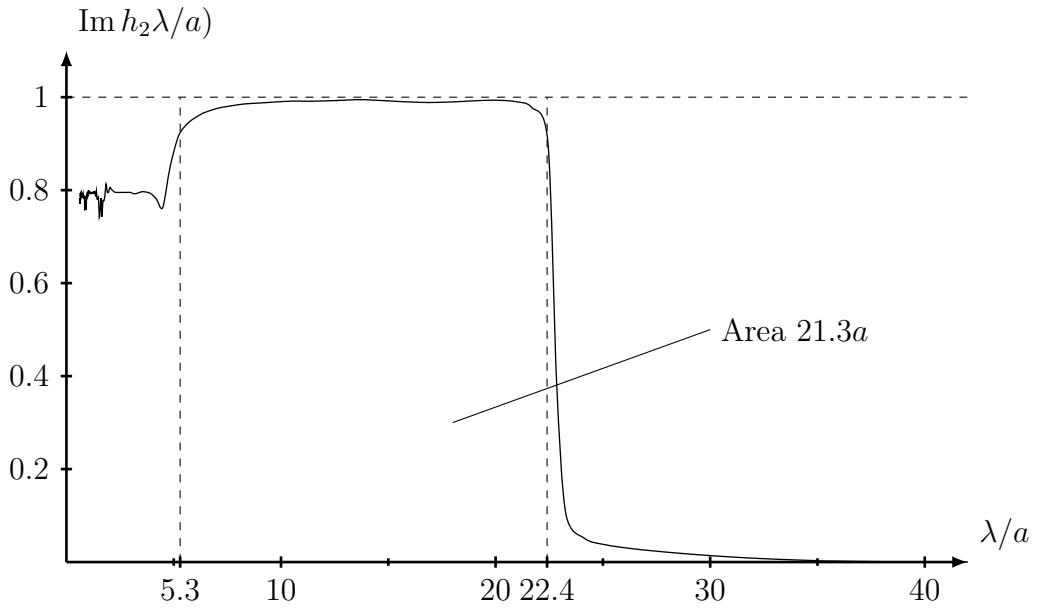

Figure 6: The function $\operatorname{Im} h_2(\lambda/a)$ for $t_0 = 0.5$ as a function of the normalized wavelength λ/a for a slab of thickness $D/a = 20$, volume fraction $\varphi = 15\%$, permittivity $\epsilon_1/\epsilon = 4$, and permeability $\mu_1/\mu = 1$.

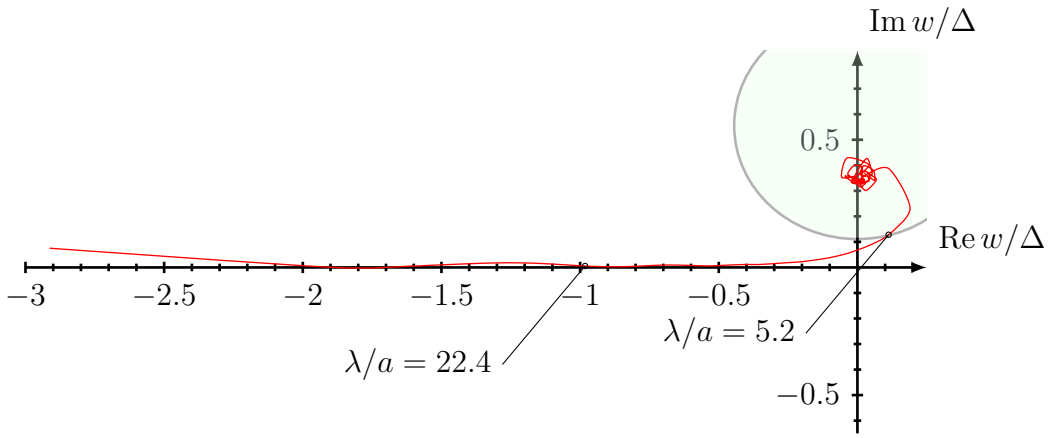

Figure 7: The components of the complex-valued w/Δ for $t_0 = 0.5$, in the complex plane as a function of the wavelength λ/a for a slab of thickness $D/a = 20$ and volume fraction $\varphi = 15\%$. The curve starts at $\lambda/a = 0$ at i/3 and ends at $-\infty + \mathrm{i}/3$ as $\lambda/a \to \infty$.

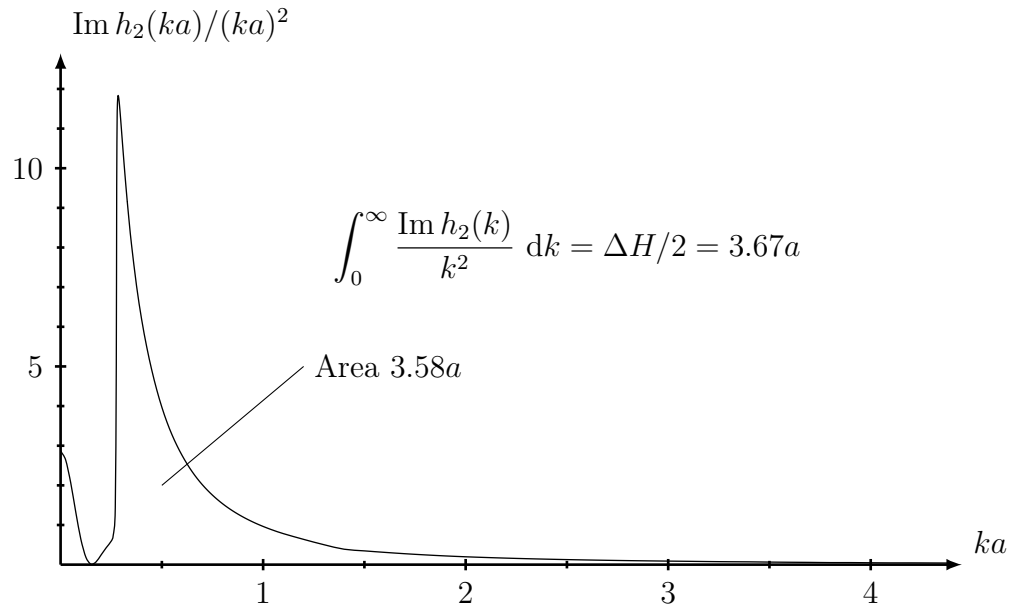

Figure 8: The function $\mathrm{Im}\, h_2(ka)/(ka)^2$ for $t_0 = 0.5$ as a function of frequency ka for a slab of thickness $D/a = 20$, volume fraction $\varphi = 15\%$, permittivity $\epsilon_1/\epsilon = 4$, and permeability $\mu_1/\mu = 1$.

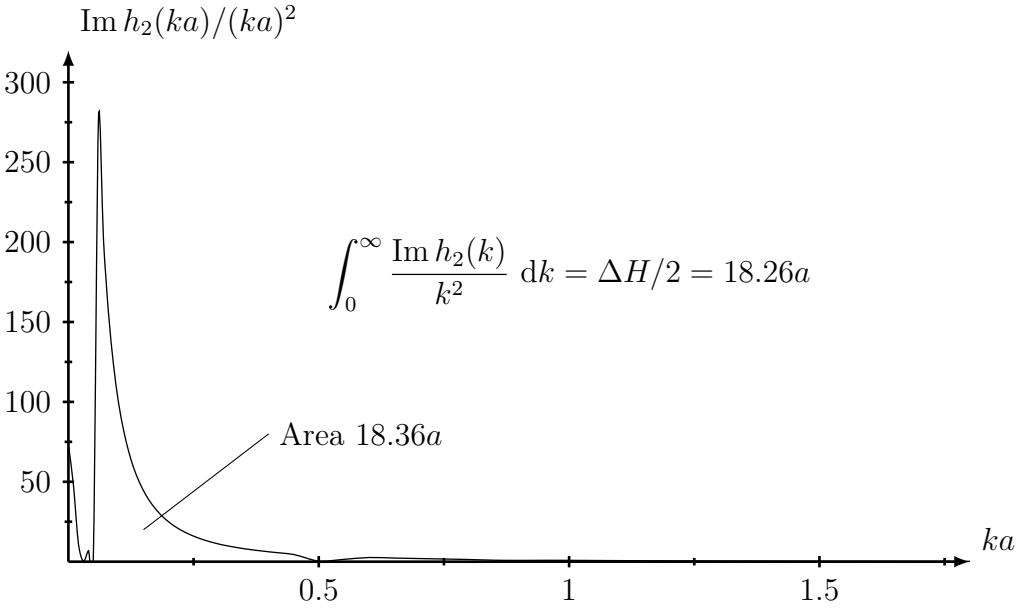

Figure 9: The function $\mathrm{Im}\, h_2(ka)/(ka)^2$ for $t_0 = 0.5$ as a function of frequency ka for a slab of thickness $D/a = 100$, volume fraction $\varphi = 15\%$, permittivity $\epsilon_1/\epsilon = 4$, and permeability $\mu_1/\mu = 1$.

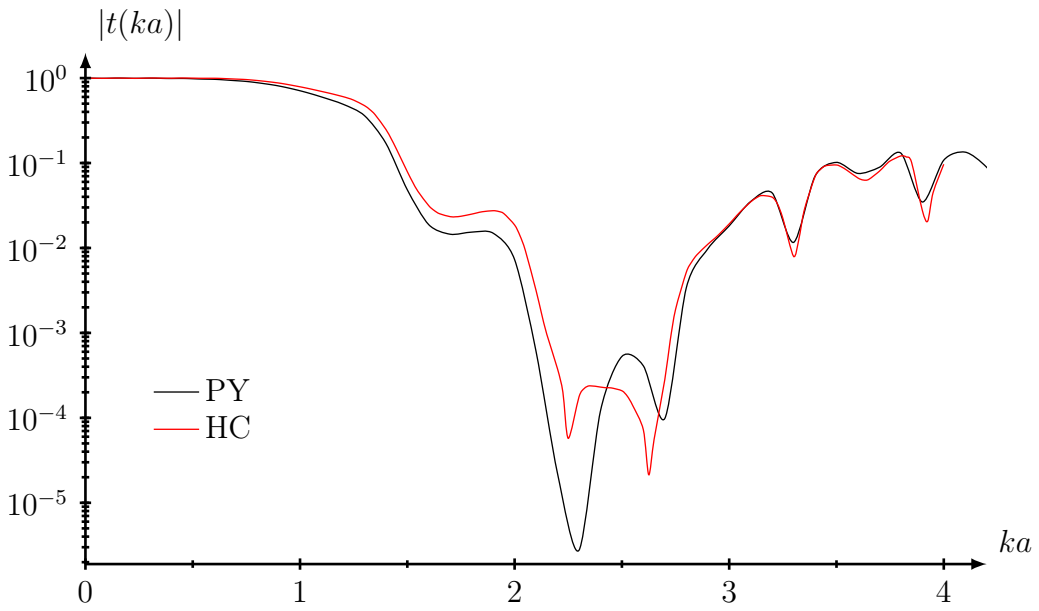

Figure 10: The transmission coefficient for the hole correction (HC) and Percus-Yevick approximation as a function of frequency ka for a slab of thickness $D/a = 20$, volume fraction $\varphi = 15\%$, permittivity $\epsilon_1/\epsilon = 4$, and permeability $\mu_1/\mu = 1$.

also serves as an independent check on the numerical precision in the numerical calculations. Numerical illustrations show that the physical bound is not obtained, which shows that these constructions are far from extreme designs. The test of numerical accuracy shows that the precision is satisfactory.

6 Acknowledgement

The analysis presented in this paper was made possible by a generous support by the Swedish Defence Research Agency, FOI. This support is gratefully acknowledged.

Appendix A The expansion coefficients

In this appendix, the coefficients $\mathcal{A}_{\tau l\tau' l'\lambda}$ are reviewed [11, 12].

$$\mathcal{A}_{\tau l\tau' l'\lambda} = -2\pi \begin{matrix} \\ \tau=1 \\ \tau=2 \end{matrix} \overset{\begin{matrix} \tau'=1 & \tau'=2 \end{matrix}}{\begin{pmatrix} C & -D \\ D & C \end{pmatrix}}$$

where

$$C = \frac{1}{2}\mathrm{i}^{l'-l+\lambda}(2\lambda+1)\sqrt{\frac{(2l+1)(2l'+1)}{l(l+1)l'(l'+1)}}$$
$$\times \begin{pmatrix} l & l' & \lambda \\ 0 & 0 & 0 \end{pmatrix} \begin{pmatrix} l & l' & \lambda \\ 1 & -1 & 0 \end{pmatrix} [l(l+1)+l'(l'+1)-\lambda(\lambda+1)]$$

$$D = \frac{1}{2}\mathrm{i}^{l'-l+\lambda+1}(2\lambda+1)\sqrt{\frac{(2l+1)(2l'+1)}{l(l+1)l'(l'+1)}}$$
$$\times \begin{pmatrix} l & l' & \lambda-1 \\ 0 & 0 & 0 \end{pmatrix} \begin{pmatrix} l & l' & \lambda \\ 1 & -1 & 0 \end{pmatrix} \sqrt{\lambda^2-(l-l')^2}\sqrt{(l+l'+1)^2-\lambda^2}$$

and where $\begin{pmatrix} \cdot & \cdot & \cdot \\ \cdot & \cdot & \cdot \end{pmatrix}$ denotes Wigner's 3j symbol [3]. Both C and D are real numbers, due to the properties of the Wigner's 3j symbol.

Appendix B Low-frequency solution

In this appendix, we solve the system of integral equations in (2.4) in the limit of small $\varepsilon = ka$ under the constraint that d/a (or D/a) is constant. Only $l = 1$ and $m = 1$ contribute in this limit. Moreover, a polarization of the incident wave in the $\hat{\boldsymbol{x}}$ direction engages only $\{\tau, \sigma\} = \{1, \mathrm{o}\}, \{2, \mathrm{e}\}$. Therefore, in the analysis, we suppress the σ, m, and l indices, and the equations to solve are [12] ($\zeta = kz, \zeta_1 = kz_1, \zeta_2 = kz_2$, $kd = \zeta_2 - \zeta_1$):

$$f_\tau(\zeta) = t_{\tau 1}a_\tau \mathrm{e}^{\mathrm{i}\zeta} + \frac{n_0 t_{\tau 1}}{k^3}\sum_{\tau'=1}^{2}\int_{\zeta_1}^{\zeta_2} K_{\tau\tau'}(\zeta-\zeta')f_{\tau'}(\zeta')\,\mathrm{d}\zeta', \quad \zeta \in [\zeta_1, \zeta_2]$$

where

$$a_{\tau 1} = -\mathrm{i}^{-\tau}\sqrt{6\pi}$$

and [11, 12]

$$K_{\tau\tau'}(\zeta) = \begin{matrix} \\ {\scriptstyle \tau=1} \\ {\scriptstyle \tau=2} \end{matrix} \begin{matrix} {\scriptstyle \tau'=1} & {\scriptstyle \tau'=2} \\ \left(\begin{matrix} 2\pi I_0(\zeta, 2\varepsilon) - \pi I_2(\zeta, 2\varepsilon) \\ 3\pi I_1(\zeta, 2\varepsilon) \end{matrix} \right. & \left. \begin{matrix} -3\pi I_1(\zeta, 2\varepsilon) \\ 2\pi I_0(\zeta, 2\varepsilon) - \pi I_2(\zeta, 2\varepsilon) \end{matrix} \right) \end{matrix}$$

The explicit values of $I_l(\zeta, \varepsilon)$, $l = 0, 1, 2$ are [11]

$$I_0(\zeta, 2\varepsilon) = \begin{cases} \mathrm{e}^{-\mathrm{i}\zeta}, & \zeta \leq -2\varepsilon \\ \mathrm{e}^{2\mathrm{i}\varepsilon}\mathrm{P}_0\left(\frac{\zeta}{2\varepsilon}\right), & -2\varepsilon < \zeta < 2\varepsilon \\ \mathrm{e}^{\mathrm{i}\zeta}, & \zeta \geq 2\varepsilon \end{cases}$$

$$I_1(\zeta, 2\varepsilon) = \begin{cases} \mathrm{i}\mathrm{e}^{-\mathrm{i}\zeta}, & \zeta \leq -2\varepsilon \\ -\mathrm{i}\mathrm{e}^{2\mathrm{i}\varepsilon}\mathrm{P}_1\left(\frac{\zeta}{2\varepsilon}\right), & -2\varepsilon < \zeta < 2\varepsilon \\ -\mathrm{i}\mathrm{e}^{\mathrm{i}\zeta}, & \zeta \geq 2\varepsilon \end{cases}$$

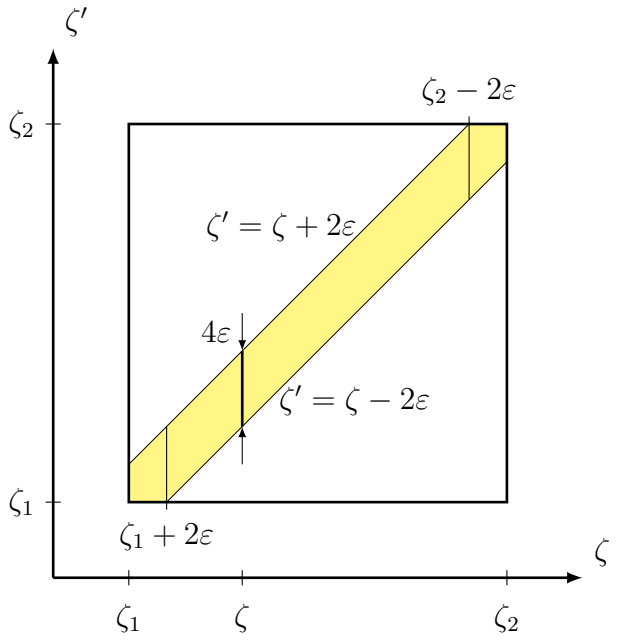

Figure 11: The domain of integration in ζ' with the hole correction in yellow.

$$I_2(\zeta, 2\varepsilon) = \begin{cases} -\mathrm{e}^{-\mathrm{i}\zeta}, & \zeta \le -2\varepsilon \\ \mathrm{e}^{2\mathrm{i}\varepsilon} \dfrac{\mathrm{i}\mathrm{P}_0\left(\frac{\zeta}{2\varepsilon}\right) - (\mathrm{i} + 2\varepsilon)\mathrm{P}_2\left(\frac{\zeta}{2\varepsilon}\right)}{2\varepsilon}, & -2\varepsilon < \zeta < 2\varepsilon \\ -\mathrm{e}^{\mathrm{i}\zeta}, & \zeta \ge 2\varepsilon \end{cases}$$

The dominant terms of the kernel in the interval (inside the hole correction) $|\zeta| \le 2\varepsilon$ are

$$K_{\tau\tau'}(\zeta) = \frac{\pi}{2\mathrm{i}\varepsilon} \begin{matrix} \tau=1 \\ \tau=2 \end{matrix} \overset{\begin{matrix} \tau'=1 & \tau'=2 \end{matrix}}{\begin{pmatrix} \mathrm{P}_0\left(\frac{\zeta}{2\varepsilon}\right) - \mathrm{P}_2\left(\frac{\zeta}{2\varepsilon}\right) + \mathcal{O}(\varepsilon) & \mathcal{O}(\varepsilon) \\ \mathcal{O}(\varepsilon) & \mathrm{P}_0\left(\frac{\zeta}{2\varepsilon}\right) - \mathrm{P}_2\left(\frac{\zeta}{2\varepsilon}\right) + \mathcal{O}(\varepsilon) \end{pmatrix}}$$

and outside the hole correction the terms are of the order $\mathcal{O}(1)$ and therefore contribute with higher orders powers in ε.

Divide the integration interval in a singular hole correction part $\zeta - \zeta' \in [-2\varepsilon, 2\varepsilon]$ and the remaining interval outside the hole correction. The integrals over the latter interval contain higher order contributions in ε and are omitted. We have to leading order

$$f_\tau(\zeta) = t_{\tau 1} a_\tau \mathrm{e}^{\mathrm{i}\zeta} + \frac{n_0 t_{\tau 1}}{k^3} \int_{|\zeta - \zeta'| \le 2\varepsilon} K_{\tau\tau}(\zeta - \zeta') f_\tau(\zeta') \, \mathrm{d}\zeta', \quad \zeta \in [\zeta_1, \zeta_2], \, \tau = 1, 2$$

where the domain of integration is depicted in yellow in Figure 11.

In the integral, we replace $f_{\tau'}(\zeta') \to f_{\tau'}(\zeta)$ — the difference contributes with higher order terms. We have

$$f_\tau(\zeta) = t_{\tau 1} a_\tau \mathrm{e}^{\mathrm{i}\zeta} + \frac{n_0 t_{\tau 1}}{k^3} f_\tau(\zeta) \int_{|\zeta - \zeta'| \le 2\varepsilon} K_{\tau\tau}(\zeta - \zeta') \, \mathrm{d}\zeta', \quad \zeta \in [\zeta_1, \zeta_2], \, \tau = 1, 2$$

Integration over the yellow area in Figure 11 contributes with

$$I_0(\zeta) = \frac{\pi}{2i\varepsilon}\int_{\zeta-2\varepsilon}^{\zeta+2\varepsilon} \mathrm{P}_0\left(\frac{\zeta-\zeta'}{2\varepsilon}\right) - \mathrm{P}_2\left(\frac{\zeta-\zeta'}{2\varepsilon}\right) \mathrm{d}\zeta' = -i\pi\int_{-1}^{1} \mathrm{P}_0(t) - \mathrm{P}_2(t)\,\mathrm{d}t$$
$$= -2i\pi, \quad \zeta_1 + 2\varepsilon \le \zeta \le \zeta_2 - 2\varepsilon$$

The two remaining parts at the ends of the slab are

$$I_1(\zeta) = \frac{\pi}{2i\varepsilon}\int_{\zeta_1}^{\zeta+2\varepsilon} \mathrm{P}_0\left(\frac{\zeta-\zeta'}{2\varepsilon}\right) - \mathrm{P}_2\left(\frac{\zeta-\zeta'}{2\varepsilon}\right) \mathrm{d}\zeta'$$
$$= -\frac{i\pi}{2}\left\{3\frac{\zeta-\zeta_1}{2\varepsilon} + 2 - \left(\frac{\zeta-\zeta_1}{2\varepsilon}\right)^3\right\}, \quad \zeta_1 \le \zeta \le \zeta_1 + 2\epsilon$$

and

$$I_2(\zeta) = \frac{\pi}{2i\varepsilon}\int_{\zeta-2\varepsilon}^{\zeta_2} \mathrm{P}_0\left(\frac{\zeta-\zeta'}{2\varepsilon}\right) - \mathrm{P}_2\left(\frac{\zeta-\zeta'}{2\varepsilon}\right) \mathrm{d}\zeta'$$
$$= -\frac{i\pi}{2}\left\{2 - 3\frac{\zeta-\zeta_2}{2\varepsilon} + \left(\frac{\zeta-\zeta_2}{2\varepsilon}\right)^3\right\}, \quad \zeta_2 - 2\varepsilon \le \zeta \le \zeta_2$$

The set of integral equations simplifies to leading order to

$$f_\tau(\zeta) = t_{\tau 1}a_\tau e^{i\zeta} + \frac{n_0 t_{\tau 1}}{k^3} f_\tau(\zeta) \begin{cases} I_1(\zeta), & \zeta_1 \le \zeta \le \zeta_1 + 2\epsilon \\ I_0(\zeta), & \zeta_1 + 2\epsilon \le \zeta \le \zeta_2 - 2\epsilon \\ I_2(\zeta), & \zeta_2 - 2\varepsilon \le \zeta \le \zeta_2 \end{cases}$$

with solutions

$$f_\tau(\zeta) = \begin{cases} \dfrac{t_{\tau 1}a_\tau e^{i\zeta}}{1 - C_\tau I_1(\zeta)}, & \zeta_1 \le \zeta \le \zeta_1 + 2\epsilon \\ \dfrac{t_{\tau 1}a_\tau e^{i\zeta}}{1 - C_\tau I_0(\zeta)}, & \zeta_1 + 2\epsilon \le \zeta \le \zeta_2 - 2\epsilon \\ \dfrac{t_{\tau 1}a_\tau e^{i\zeta}}{1 - C_\tau I_2(\zeta)}, & \zeta_2 - 2\varepsilon \le \zeta \le \zeta_2 \end{cases}$$

where the constant C_τ is

$$C_\tau = \frac{n_0 t_{\tau 1}}{k^3} = \frac{3\varphi t_{\tau 1}}{4\pi\varepsilon^3}\frac{D}{d}$$

Finally, we can calculate y_τ for $l = 1$.

$$\begin{aligned} y_\tau &= \int_{\zeta_1}^{\zeta_2} f_\tau(\zeta) \mathrm{e}^{-\mathrm{i}\zeta}\, \mathrm{d}\zeta \\ &= -\mathrm{i}^{-\tau} t_{\tau 1} \sqrt{6\pi} \left(\int_{\zeta_1}^{\zeta_1+2\varepsilon} \frac{\mathrm{d}\zeta}{1 - C_\tau I_1(\zeta)} + \frac{kd - 4\varepsilon}{1 + 2\mathrm{i}\pi C_\tau} + \int_{\zeta_2-2\varepsilon}^{\zeta_2} \frac{\mathrm{d}\zeta}{1 - C_\tau I_2(\zeta)} \right) \\ &= -\mathrm{i}^{-\tau} t_{\tau 1} \sqrt{6\pi} \left(\frac{kd - 4\varepsilon}{1 + 2\mathrm{i}\pi C_\tau} + 4\varepsilon \int_0^1 \frac{\mathrm{d}t}{1 + \frac{\mathrm{i}\pi}{2} C_\tau \left(2 + 3t - t^3\right)} \right) \\ &= -\mathrm{i}^{-\tau} t_{\tau 1} \sqrt{6\pi} \varepsilon \left(\frac{d/a}{1 + 2\mathrm{i}\pi C_\tau} + A_\tau^{\mathrm{Corr}} \right) \end{aligned}$$

where the correction term A_τ^{Corr} is

$$A_\tau^{\mathrm{Corr}} = 4 \int_0^1 \frac{\mathrm{d}t}{1 + \frac{\mathrm{i}\pi}{2} C_\tau \left(2 + 3t - t^3\right)} - \frac{4}{1 + 2\mathrm{i}\pi C_\tau}$$

The remaining integral can be solved analytically by finding the roots of the denominator and a partial fraction of the integrand.

$$\begin{aligned} \int_0^1 \frac{\mathrm{d}t}{a + 3t - t^3} &= \int_0^1 \frac{\mathrm{d}t}{(t - a_1)(t - a_2)(t - a_3)} \\ &= \sum_{n=1}^{3} \int_0^1 \frac{A_n\, \mathrm{d}t}{t - a_n} = \sum_{n=1}^{3} A_n \ln \frac{a_n - 1}{a_n} \end{aligned}$$

where a_n, $n = 1, 2, 3$ are the roots of the denominator, and

$$A_1 = \frac{1}{(a_1 - a_2)(a_1 - a_3)}, \quad A_2 = \frac{1}{(a_2 - a_1)(a_2 - a_3)}, \quad A_3 = \frac{1}{(a_3 - a_1)(a_3 - a_2)}$$

In an numerical illustration, it is more convenient to numerically compute the integral than to try to find the analytic solution.

The constant H can now be determined from the low-frequency limit of the transmission coefficient in (2.1). The result is

$$\begin{aligned} H = \frac{2\pi n_0}{\mathrm{i}k^4} \sum_{\tau=1}^{2} \mathrm{i}^{\tau-2} \sqrt{\frac{3}{8\pi}} y_\tau &= \frac{3\pi n_0}{\mathrm{i}k^4} \sum_{\tau=1}^{2} t_{\tau 1} \varepsilon \left(\frac{d/a}{1 + 2\mathrm{i}\pi C_\tau} + A_\tau^{\mathrm{Corr}} \right) \\ &= -3\mathrm{i}\pi a \sum_{\tau=1}^{2} C_\tau \left(\frac{d/a}{1 + 2\mathrm{i}\pi C_\tau} + A_\tau^{\mathrm{Corr}} \right) = H^{\mathrm{Appr}} + H^{\mathrm{Corr}} \end{aligned}$$

where

$$\begin{cases} H^{\mathrm{Appr}} = -3\mathrm{i}\pi \sum\limits_{\tau=1}^{2} \dfrac{C_\tau d}{1+2\mathrm{i}\pi C_\tau} = -9\mathrm{i}\varphi D \sum\limits_{\tau=1}^{2} \dfrac{t_{\tau 1}}{4\varepsilon^3 + 6\mathrm{i}\varphi t_{\tau 1}\frac{D}{d}} \\ H^{\mathrm{Corr}} = -3\mathrm{i}\pi a \sum\limits_{\tau=1}^{2} C_\tau A_\tau^{\mathrm{Corr}} \\ \qquad = -36\mathrm{i}\varphi \dfrac{D}{d} a \sum\limits_{\tau=1}^{2} \left(\int_0^1 \dfrac{t_{\tau 1}\,\mathrm{d}t}{4\varepsilon^3 + \frac{3\mathrm{i}}{2}\varphi t_{\tau 1}\frac{D}{d}(2+3t-t^3)} - \dfrac{t_{\tau 1}}{4\varepsilon^3 + 6\mathrm{i}\varphi t_{\tau 1}\frac{D}{d}} \right) \end{cases} \tag{B.1}$$

Appendix C Titchmarsh's theorem

The Titchmarsh's theorem is used in this paper and for convenience, we state the theorem in this appendix [21]. Parts of this theorem is related to the Paley-Wiener theorem.

Theorem C.1 (Titchmarsh)**.** *Denote the Fourier transform of the function $f(t)$ by $\hat{f}(\omega)$. If $\hat{f}(\omega)$ is square integrable on the real axis, i.e., $\hat{f} \in L^2(\mathbb{R})$, the following three conditions are equivalent:*

1. *The inverse Fourier transform $f(t)$ of $\hat{f}(\omega)$ vanishes for $t<0$, i.e.,*

$$f(t) = \int_{-\infty}^{\infty} \hat{f}(\omega)\mathrm{e}^{-\mathrm{i}\omega t}\,\mathrm{d}x = 0, \quad t<0$$

2. *$\hat{f}(\omega)$ is, for almost all ω, the limit as $\zeta \to 0^+$ of an analytic function $\hat{f}(\omega+\mathrm{i}\zeta)$, which is holomorphic in the upper half-plane and satisfies*

$$\int_{-\infty}^{\infty} |\hat{f}(\omega+\mathrm{i}\zeta)|^2\,\mathrm{d}\omega < \infty, \quad \zeta>0$$

3. *The real and imaginary parts of $\hat{f}(\omega) = \hat{f}_{\mathrm{r}}(\omega)+\mathrm{i}\hat{f}_{\mathrm{i}}(\omega)$ satisfy Plemelj's formulas*

$$\begin{cases} \hat{f}_{\mathrm{r}}(\omega) = \dfrac{1}{\pi} \fint_{-\infty}^{\infty} \dfrac{\hat{f}_{\mathrm{i}}(\omega')}{\omega'-\omega}\,\mathrm{d}\omega' \\ \hat{f}_{\mathrm{i}}(\omega) = -\dfrac{1}{\pi} \fint_{-\infty}^{\infty} \dfrac{\hat{f}_{\mathrm{r}}(\omega')}{\omega'-\omega}\,\mathrm{d}\omega' \end{cases}$$

Appendix D Herglotz functions and integral identity

In this appendix, we investigate the Herglotz functions and some integral identities with these functions. More technical details can be found in [1, 14, 20, 26].

A Herglotz function is defined as [20]

Definition D.1. *A function $h(z)$ is called a Herglotz function if*

1. *$h(z)$ is defined and analytic everywhere in the upper complex half-plane, $\mathbb{C}_+ = \{z \in \mathbb{C} : \operatorname{Im} z > 0\}$*
2. *$\operatorname{Im} h(z) \geq 0$ for all $z \in \mathbb{C}_+$*

If $h(z)$ is a Herglotz function, then $-1/h(z)$ is a Herglotz function, and if $h(z)$ and $g(z)$ are Herglotz functions, the composition $h(g(z))$ is a new Herglotz function, provided $g(z)$ does not attain real values for $z \in \mathbb{C}_+$.

We adopt the following definitions [20]:

Definition D.2. *If the Herglotz function $h(z)$ satisfies $h(-z^*) = -h^*(z)$, $z \in \mathbb{C}_+$, the Herglotz function is symmetric.*

Definition D.3. *If for $N \geq -1$, the Herglotz function $h(z)$ satisfies*

$$h(z) = \sum_{n=-1}^{N} b_{-n} z^{-n} + o\left(z^{-N}\right), \qquad \text{as } z \hat{\to} \infty$$

*where the constants b_{-n}, $n = -1, 0, \ldots, N$ are all **real**, then $h(z)$ admits at $z = \infty$ an asymptotic expansion of order N. The symbol $z \hat{\to} \infty$ stands for the non-tangential limit $|z| \to \infty$ within some Stoltz domain $\{z \in \mathbb{C}_+ : \theta \leq \arg(z) \leq \pi - \theta\}$ with the angle $\theta \in (0, \pi/2]$.*

Definition D.4. *If for $N \geq -1$, the Herglotz function $h(z)$ satisfies*

$$h(z) = \sum_{n=-1}^{N} a_n z^n + o\left(z^{N}\right), \qquad \text{as } z \hat{\to} 0$$

*where the constants a_n, $n = -1, 0, \ldots, N$ are all **real**, then $h(z)$ admits at $z = 0$ an asymptotic expansion of order N. The notation $z \hat{\to} 0$ stands for the non-tangential limit $|z| \to 0$ within some Stoltz domain $\{z \in \mathbb{C}_+ : \theta \leq \arg(z) \leq \pi - \theta\}$ with the angle $\theta \in (0, \pi/2]$.*

The following two theorems are instrumental [1]:

Theorem D.1. *Let $h(z)$ be a Herglotz function. Then for some integer $N_\infty \geq 0$ the following integral*

$$\lim_{\varepsilon \to 0^+} \lim_{y \to 0^+} \int_{\varepsilon < x < 1/\varepsilon} x^{2N_\infty} \operatorname{Im} h(x + \mathrm{i}y) \, \mathrm{d}x$$

exists as a finite number if and only if $h(z)$ admits an asymptotic expansion of order $2N_\infty + 1$ at $z = \infty$. In this case

$$\lim_{\varepsilon \to 0^+} \lim_{y \to 0^+} \frac{1}{\pi} \int_{\varepsilon < x < 1/\varepsilon} x^{n} \operatorname{Im} h(x + \mathrm{i}y) \, \mathrm{d}x = \begin{cases} a_{-1} - b_{-1}, & n = 0 \\ -b_{-n-1}, & 0 < n \leq 2N_\infty \end{cases}$$

holds.

Theorem D.2. *Let $h(z)$ be a Herglotz function. Then for some integer $N_0 \geq 1$ the following integral*

$$\lim_{\varepsilon\to 0^+}\lim_{y\to 0^+}\int_{\varepsilon<x<1/\varepsilon}\frac{\operatorname{Im} h(x+\mathrm{i}y)}{x^{2N_0}}\,\mathrm{d}x$$

exists as a finite number if and only if $h(z)$ admits an asymptotic expansion of order $2N_0-1$ at $z=0$. In this case

$$\lim_{\varepsilon\to 0^+}\lim_{y\to 0^+}\frac{1}{\pi}\int_{\varepsilon<x<1/\varepsilon}\frac{\operatorname{Im} h(x+\mathrm{i}y)}{x^{n}}\,\mathrm{d}x=\begin{cases}a_1-b_1, & n=2\\ a_{n-1}, & 2<n\leq 2N_0\end{cases}$$

holds.

Appendix E The pulse Herglotz function

In this appendix we analyze the pulse Herglotz function.[6]

$$h(z)=-\frac{1}{\pi}\int_{-1}^{1}\frac{1}{z-t}\,\mathrm{d}t=\frac{1}{\pi}\ln\frac{z-1}{z+1},\quad \operatorname{Im} z>0$$

where the branch cut of the logarithm is assumed along the negative real axis (principal branch cut, $-\pi<\arg z\leq\pi$).

We focus on the imaginary part of this function in the upper complex half plane, $z=x+\mathrm{i}y$, $y>0$.

$$\operatorname{Im} h(z)=\frac{1}{\pi}\arg\frac{z-1}{z+1}$$

Points $z=x+\mathrm{i}y$ with constant phase θ of the expression $(z-1)/(z+1)$ satisfy

$$\tan\theta=\frac{2y}{x^2+y^2-1},\quad \theta\in[0,\pi]$$

This is the equation of a circle with center $z_0=x_0+\mathrm{i}y_0$ and radius r, where

$$\begin{cases}x_0=0\\ y_0=\dfrac{1}{\tan\theta}\\ r=\sqrt{\dfrac{1}{\tan^2\theta}+1}\end{cases}\qquad \operatorname{Im} h(z)=\theta/\pi$$

The imaginary part of $h(z)$ is bounded by unity in the upper complex half plane, $0\leq\operatorname{Im} h(z)\leq 1$. Moreover, inside the unit circle ($\pi/2<\theta<\pi$, see Figure 12) in

[6] An alternative expression of the pulse Herglotz function is [22]

$$h(z)=\mathrm{i}-\frac{2}{\pi}\operatorname{arctanh}(z),\quad z\in\mathbb{C}\setminus(-\infty,-1]\cup[1,\infty)$$

where the values on the real axis are taken as limits as $y\to 0^+$ (upper side of the branch cuts).

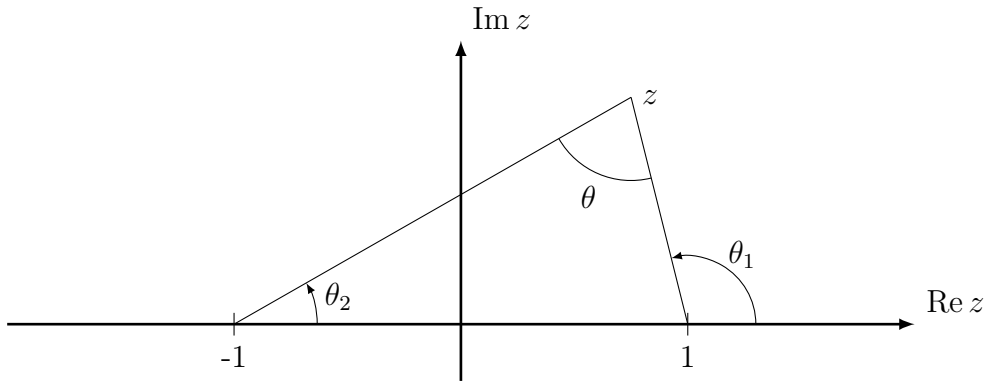

Figure 12: The argument $\arg z = \theta = \theta_1 - \theta_2$ as a function of the angles θ_1 and θ_2.

the upper complex half plane, $1/2 < \operatorname{Im} h(z) < 1$, see Figure 13. On the real axis $z = x$ we have, see Figure 14

$$\operatorname{Im} h(z) = \begin{cases} 1, & -1 < x < 1 \\ 0, & (-\infty, -1) \cup [1, \infty) \end{cases}$$

The asymptotes of $h(z)$ are

$$h(z) = \begin{cases} \mathrm{i} - \dfrac{2z}{\pi} + O(z^2), & z \hat{\to} 0 \\ -\dfrac{2}{z\pi} + O(z^{-2}), & z \hat{\to} \infty \end{cases}$$

We also notice that $h(z)$ is a symmetric Herglotz function. In fact, for the principal branch, we have outside the branch cut

$$\ln(z^*) = (\ln z)^*, \quad \ln \frac{1}{z} = -\ln z$$

which leads to

$$h(-z^*) = \frac{1}{\pi} \ln \frac{z^* + 1}{z^* - 1} = \left(\frac{1}{\pi} \ln \frac{z+1}{z-1} \right)^* = -\left(\frac{1}{\pi} \ln \frac{z-1}{z+1} \right)^* = -h^*(z), \quad z \in \mathbb{C}_+$$

References

[1] A. Bernland, A. Luger, and M. Gustafsson. Sum rules and constraints on passive systems. *J. Phys. A: Math. Theor.*, **44**(14), 145205, 2011.

[2] C. R. Brewitt-Taylor. Limitation on the bandwidth of artificial perfect magnetic conductor surfaces. *Microwaves, Antennas & Propagation, IET*, **1**(1), 255–260, 2007.

[3] A. R. Edmonds. *Angular Momentum in Quantum Mechanics*. Princeton University Press, Princeton, NJ, 3 edition, 1974.

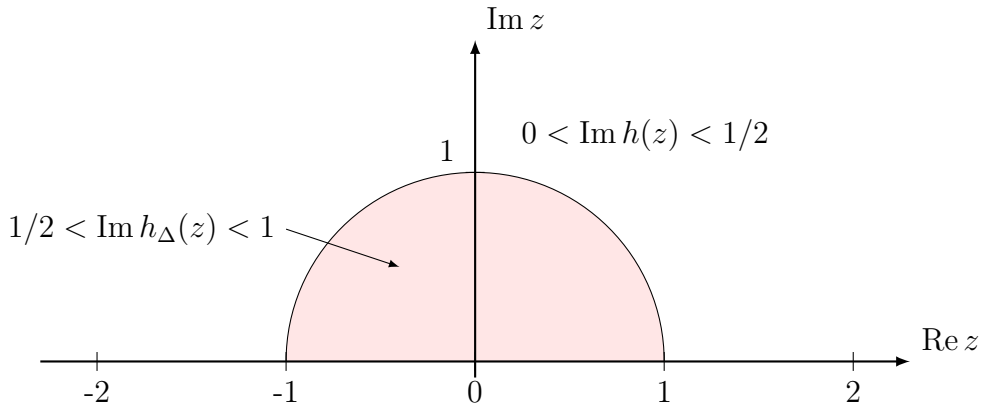

Figure 13: The value of the imaginary part of the function $h(x)$ in the upper complex half plane.

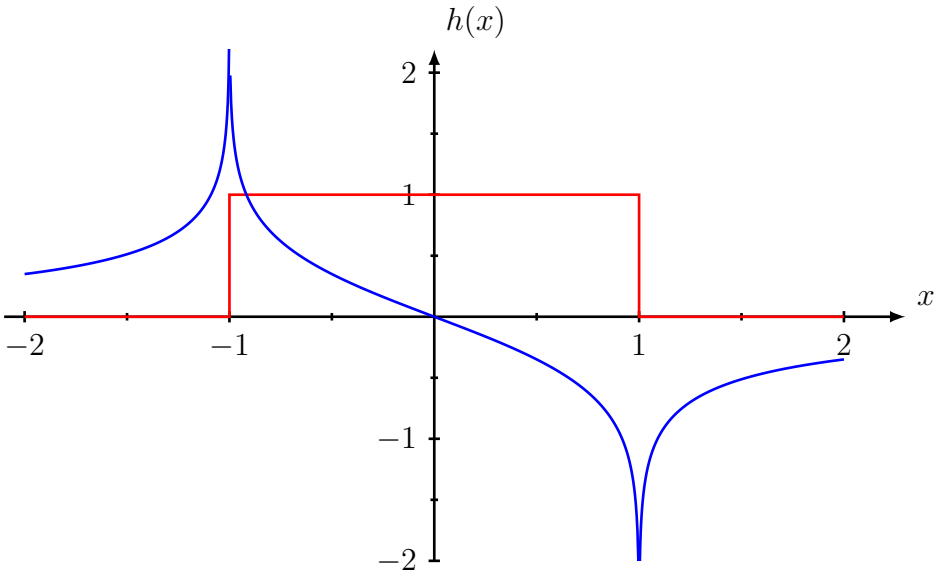

Figure 14: The function $\mathrm{Re}\, h(x)$ (blue curve) and $\mathrm{Im}\, h(x)$ (red curve) for a real argument x.

[4] M. Gustafsson and D. Sjöberg. Sum rules and physical bounds on passive metamaterials. *New Journal of Physics*, **12**, 043046, 2010.

[5] M. Gustafsson, C. Sohl, and G. Kristensson. Physical limitations on antennas of arbitrary shape. *Proc. R. Soc. A*, **463**, 2589–2607, 2007.

[6] M. Gustafsson and D. Sjöberg. Physical Bounds and Sum Rules for High-Impedance Surfaces. *IEEE Trans. Antennas Propag.*, **59**(6), 2196–2204, 2011.

[7] M. Gustafsson, C. Sohl, C. Larsson, and D. Sjöberg. Physical bounds on the all-spectrum transmission through periodic arrays. *Europhysics Letters*, **87**(3), 34002, 2009.

[8] M. Gustavsson, G. Kristensson, and N. Wellander. Multiple scattering by a collection of randomly located obstacles. Part II: Numerical implementation — coherent fields. Technical Report LUTEDX/(TEAT-7236)/1–19/(2014), Revision No. 1, January 2021, Lund University, Department of Electrical and Information Technology, P.O. Box 118, S-221 00 Lund, Sweden, 2014.

[9] M. Gustavsson, G. Kristensson, and N. Wellander. Multiple scattering by a collection of randomly located obstacles — numerical implementation of the coherent fields. *J. Quant. Spectrosc. Radiat. Transfer*, **185**, 95–100, 2016.

[10] P. Henrici. *Applied and Computational Complex Analysis*, volume 1. John Wiley & Sons, New York, NY, 1974.

[11] G. Kristensson. Multiple scattering by a collection of randomly located obstacles. Part I: Theory — coherent fields. Technical Report LUTEDX/(TEAT-7235)/1–49/(2014), Lund University, Department of Electrical and Information Technology, P.O. Box 118, S-221 00 Lund, Sweden, 2014.

[12] G. Kristensson. Coherent scattering by a collection of randomly located obstacles — an alternative integral equation formulation. *J. Quant. Spectrosc. Radiat. Transfer*, **164**, 97–108, 2015.

[13] G. Kristensson. Evaluation of some integrals relevant to multiple scattering by randomly distributed obstacles. *Journal of Mathematical Analysis and Applications*, **432**(1), 324–337, 2015.

[14] G. Kristensson. *Scattering of Electromagnetic Waves by Obstacles*. Mario Boella Series on Electromagnetism in Information and Communication. SciTech Publishing, Edison, NJ, USA, 2016.

[15] G. Kristensson. Multiple scattering by a collection of randomly located obstacles. Part V: Low order contributions to the coherent fields. Technical Report LUTEDX/(TEAT-7277)/1–45/(2023), Lund University, Department of Electrical and Information Technology, P.O. Box 118, S-221 00 Lund, Sweden, 2023.

[16] G. Kristensson, M. Gustavsson, and N. Wellander. Multiple scattering by a collection of randomly located obstacles. Part IV: The effect of the pair correlation function. Technical Report LUTEDX/(TEAT-7272)/1–23/(2021), Lund University, Department of Electrical and Information Technology, P.O. Box 118, S-221 00 Lund, Sweden, 2021.

[17] G. Kristensson, M. Gustavsson, and N. Wellander. The coherent electromagnetic field and the effect of the pair distribution function. *J. Quant. Spectrosc. Radiat. Transfer*, **285**, 108178, 2022.

[18] G. Kristensson and N. Wellander. Multiple scattering by a collection of randomly located obstacles distributed in a dielectric slab. In K. Kobayashi and P. D. Smith, editors, *Advances in Mathematical Methods for Electromagnetics*, chapter 25, pages 621–651. SciTech Publishing, 2021.

[19] A. Ludvig-Osipov, J. Lundgren, C. Ehrenborg, Y. Ivanenko, A. Ericsson, M. Gustafsson, B. L. G. Jonsson, and D. Sjöberg. Fundamental Bounds on Transmission Through Periodically Perforated Metal Screens With Experimental Validation. *IEEE Transactions on Antennas and Propagation*, **68**(2), 773–782, 2020.

[20] M. Nedic, C. Ehrenborg, Y. Ivanenko, A. Ludvig-Osipov, S. Nordebo, A. Luger, L. Jonsson, D. Sjöberg, and M. Gustafsson. Herglotz functions and applications in electromagnetics. In K. Kobayashi and P. D. Smith, editors, *Advances in Mathematical Methods for Electromagnetics*, chapter 20, pages 491–514. Institution of Engineering and Technology, UK, 2021.

[21] H. M. Nussenzveig. *Causality and dispersion relations.* Academic Press, London, 1972.

[22] F. W. J. Olver, D. W. Lozier, R. F. Boisvert, and C. W. Clark. *NIST Handbook of mathematical functions.* Cambridge University Press, New York, 2010.

[23] K. N. Rozanov. Ultimate thickness to bandwidth ratio of radar absorbers. *IEEE Trans. Antennas Propag.*, **48**(8), 1230–1234, August 2000.

[24] W. Rudin. *Real and Complex Analysis.* McGraw-Hill, New York, NY, 1987.

[25] C. Sohl, M. Gustafsson, and G. Kristensson. Physical limitations on broadband scattering by heterogeneous obstacles. *J. Phys. A: Math. Theor.*, **40**, 11165–11182, 2007.

[26] C. Sohl, M. Gustafsson, G. Kristensson, and S. Nordebo. A general approach for deriving bounds in electromagnetic theory. In *Proceedings of the XXIXth URSI General Assembly*, page B01p4, Chicago, IL, USA, August 7–16 2008. International Union of Radio Science.